BIOPHYSICS

Surface-induced flow: A natural microscopic engine using infrared energy as fuel

Zheng Li* and Gerald H. Pollack*

Fluid commonly flows in response to an external pressure gradient. However, when a tunnel-containing hydrogel is immersed in water, spontaneous flow occurs through the tunnel without any pressure gradient. We confirmed this flow in a wide range of plant- and animal-derived hydrogels. The flow appears to be driven by axial concentration gradients originating from surface activities of the tunnel wall. Those activities include (i) hydrogel-water interaction and (ii) material exchange across the tunnel boundary. Unlike pressure-driven flow, this surface-induced flow has two distinct features: incident infrared energy substantially increases flow velocity, and narrower tunnels generate faster flow. Thus, surface activities in hydrogel-lined tunnels may confer kinetic energy on the enclosed fluid, with infrared as an energy source.

INTRODUCTION

Tubular flows are common natural phenomena. Examples include blood and lymphatic flows in animals and xylem and phloem flows in plants. These flows serve two main functions: fluid transport and material exchange. The principal driving force for flow is widely considered to be a pressure gradient, driving the fluid either by propulsion (cardiac contraction) or by suction (capillary effect, drawing water to the tops of plants) (*1*–*3*).

While fluid certainly flows in response to a driving force, a pressure gradient is not necessarily the only possible driver. Recently, we discovered an intratubular flow that occurs in the absence of any pressure gradient (*4*, *5*). This unexpected phenomenon was observed while studying features of the exclusion zone, or "EZ"—a molecularly ordered aqueous region next to various hydrophilic surfaces that profoundly excludes particles and solutes (*6*–*13*).

EZs were studied previously by immersing sections of tubes made of a strongly hydrophilic material, Nafion, in aqueous microsphere suspensions. A microsphere-free EZ developed adjacent to the tube surface. In the central core of the tube, the movement of the microspheres demonstrated a flow, continuously sustaining itself at a velocity of ~10 μm/s in the axial direction. Similarly, EZ and flow were also observed in tunnels lodged within various hydrogels. The gel materials included polyethylene glycol, poly(vinyl alcohol), and poly(acrylic acid) (*4*, *5*). On the other hand, flow was not observed in tubes built of hydrophobic materials such as Teflon, which do not generate EZs (*4*). The presence of EZ appeared to be a necessary condition.

The EZ is generally negatively charged, whereas the region beyond is commonly positively charged (*7*, *9*, *14*). Incident radiation energy fuels EZ, with infrared radiation (IR) being the most effective wavelength (*15*). We hypothesized that EZ and consequent flow arise from an interaction at the material-water interface (*4*, *5*, *16*), although other hypotheses are possible (*17*–*19*). After absorbing incident radiant energy, water molecules at the interfacial region break apart (as in the first step of photosynthesis) (*15*). The OH^- groups coalesce to form the EZ, a highly ordered, negatively charged zone, forming adjacent to the interface, while the complementary H^+ components are released into the core of the tube. The core thereby acquires high positive charge. That positive charge creates a gradient with the uncharged external bath beyond the tube's exits, driving a flow down the gradient, one way or the other depending on which end dominates (*5*). We referred to this phenomenon as "self-driven flow."

Since incident radiant energy (light) fuels EZ expansion, that energy may likewise fuel the self-driven flow. We confirmed that application of ultraviolet-containing white light could boost flow velocity by up to 500% (*5*). Thus, the self-driven flow mechanism can convert radiant energy into kinetic energy.

Several questions arise: (i) Is the self-driven flow an exclusive feature of certain tubular materials or a more general feature in materials occurring in nature? (ii) Among optical wavelengths, IR has shown the highest capability of expanding the EZ (*15*); could the environmentally abundant infrared energy serve as fuel for the self-driven flow? (iii) Material exchange across the wall is a common feature of naturally occurring vessels, such as capillaries. The rate of exchange may vary along the vessel, resulting in axial material concentration gradients. If proton gradients can drive flow, could other concentration gradients also drive flow?

RESULTS

Generality of self-driven flow

To explore the generality of the self-driven flow, we tested diverse hydrogels. They comprised plant-derived hydrogels including agarose, agar, and starch, as well as animal-derived hydrogels including collagen and gelatin. These hydrogels, ranging from polysaccharides to proteins, were chosen on the basis of their broad appearance in nature and wide application in science and technology (*20*–*23*).

We first tested for the presence of EZs lining the exteriors of those gels. A microsphere suspension was prepared by mixing deionized (DI) water and 1-μm nonfunctionalized polystyrene microspheres (volume ratio, 300:1). A piece of hydrogel material was fully immersed in this suspension, and the interfacial region was examined microscopically after some minutes for the presence of microsphere-free regions (EZs).

EZ presence was confirmed with all materials tested (Fig. 1). For generating the largest EZs, we found that low ion concentration inside the gel and limited tendency to absorb water were key. Standard preparations of collagen contain extraneous ions (*24*), and gelatin

Department of Bioengineering, University of Washington, Seattle, WA, USA.
*Corresponding author. Email: zhl@u.washington.edu (Z.L.); ghp@u.washington.edu (G.H.P.)

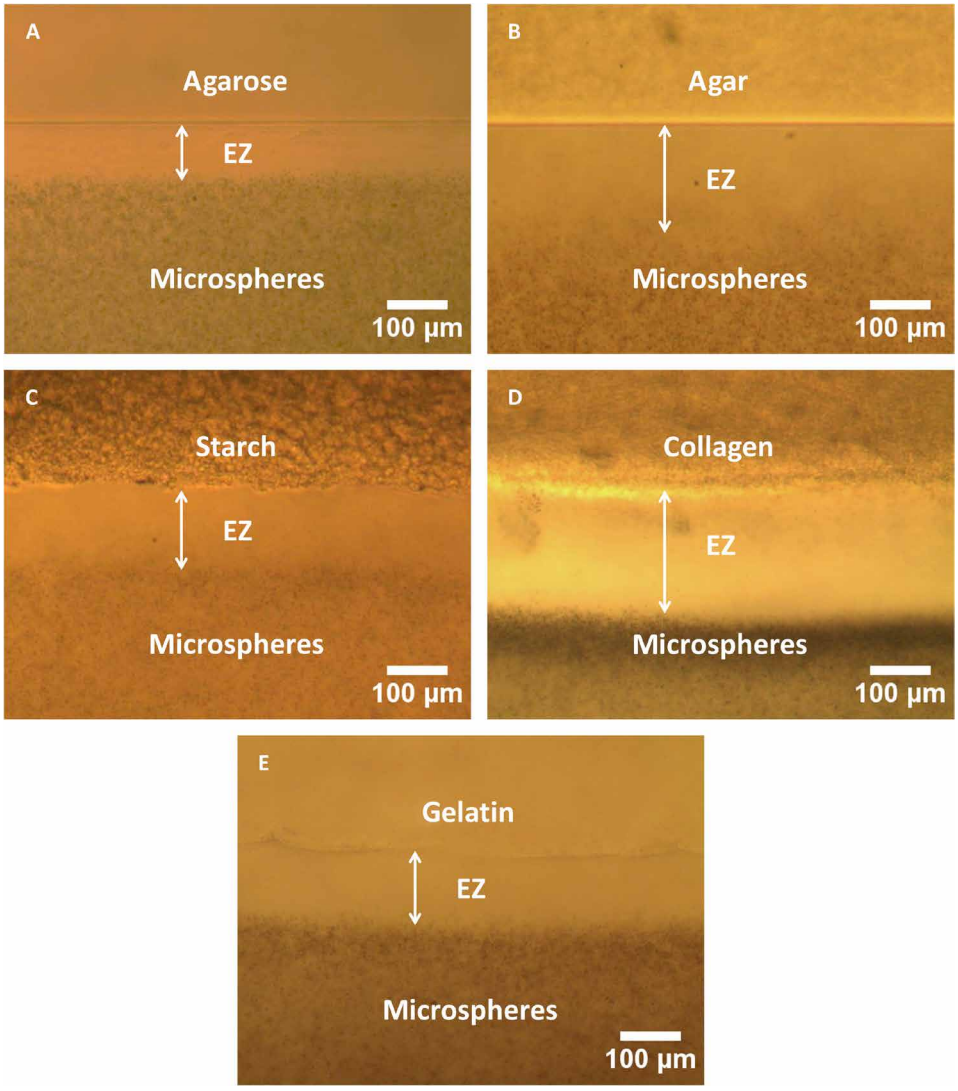

Fig. 1. EZs formed next to various hydrogels. (**A**) Agarose, (**B**) agar, (**C**) starch, (**D**) collagen (dialyzed), and (**E**) gelatin (dialyzed).

has an appreciable tendency to absorb water. When those two gels were freshly made, EZs were not observed. Dialyzing against DI water removed ions and fully hydrated the gel. After dialysis, EZs appeared clearly. For starch, agar, and agarose, EZs were readily visible without dialysis, although dialyzing those hydrogels against DI water could increase EZ size.

The generality of the EZ phenomenon was tested also with various types of particles. They included polystyrene microspheres with positive or negative functional groups, silica microspheres, polydimethylsiloxane (PDMS) beads, diatomaceous earth, and active charcoal powder. All were excluded (fig. S4). Hence, EZ is an exclusive feature neither of certain hydrogels nor of certain types of microspheres.

With the confirmed presence of EZ in all cases, we proceeded to build tunnels within the respective hydrogels to study the self-driven flow. The tunnels were fabricated by molding. The liquefied hydrogel was injected into a case, which contained a removable mold (Fig. 2A). After the gel had solidified (Fig. 2B), the mold was removed, leaving the tunnel behind (Fig. 2C). We built tunnels with asymmetric geometry: either a stepwise tunnel composed of a narrower section in series with a wider section or a tapered tunnel. The asymmetry was designed to help determine the basis underlying the flow direction.

To observe the flow, the tunnel was first filled with an aqueous microsphere suspension to eliminate air-water interface, which may cause unwanted capillary effects. Then, the entire gel tunnel was fully immersed in the microsphere suspension bath, and the exposed surface of the gel was covered with a coverslip, ready for flow observations (Fig. 2D). The flow was determined by tracking the movement of the microspheres, which was recorded by a video camera mounted on a microscope and later analyzed by particle image velocimetry (PIV) (Fig. 2E). As a negative control, we built the tunnel inside the hydrophobic material PDMS, in which neither an EZ nor any self-driven flow was expected.

Features of self-driven flow

Self-driven flow was confirmed with all the hydrogels tested (movies S1 to S5). The flow velocity differed by tunnel material and geometry but consistently met the criterion for self-driven flow, i.e., higher

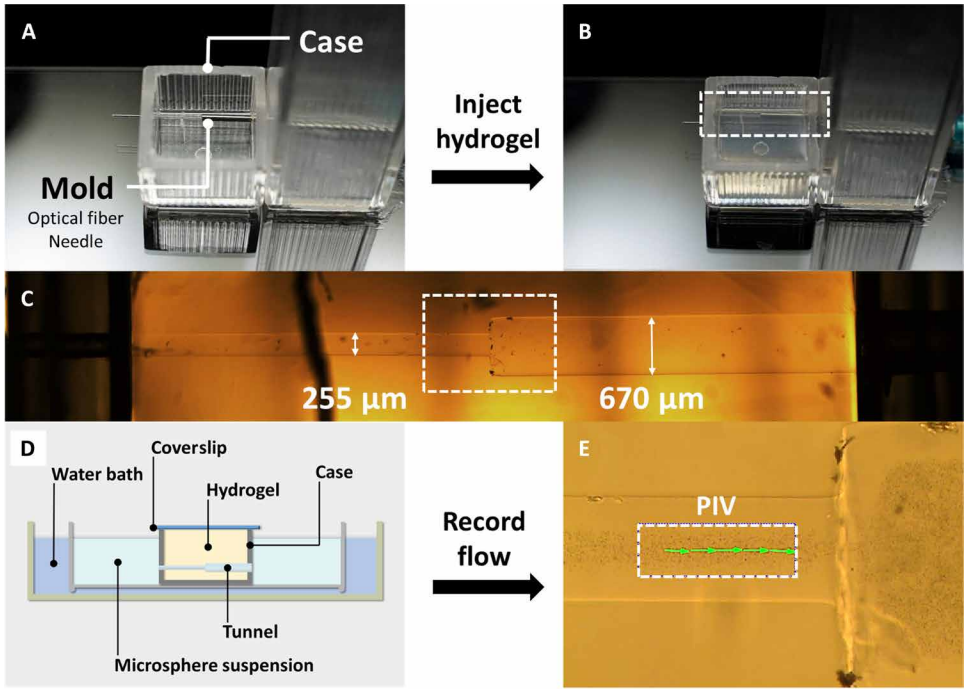

Fig. 2. Tunnel fabrication and data acquisition. (**A**) Case and mold. The case was made from a polystyrene cuvette, and the mold was made of a linear combination of optical fiber and stainless steel needle. Other molds were used as well (fig. S1). (**B**) Hydrogel material (agarose) was injected into the mold and allowed to cure. (**C**) A representative tunnel (agarose) seen under a 5× objective lens. Flow in the junction region (white dashed rectangle) was recorded by a video camera as raw data. (**D**) A side view of the experimental setup for observing the flow. The tunnel was filled with, and then immersed in, a microsphere suspension. The tunnel remained in the case, and the top surface of the hydrogel was covered with a coverslip. The level of microsphere suspension was set above both ends of the tunnel. A water bath, heated by a heating stage, provided infrared radiation energy when needed. (**E**) The flow was visualized by the movement of microspheres (black dots). The white dashed rectangle shows region of interest (ROI). Flow velocity at the ROI was quantified using particle image velocimetry (PIV). The green arrows are sample results. Arrow orientation denotes flow direction; arrow length denotes the local flow velocity.

than 0.5 µm/s, which is the root mean square speed of 1-µm Brownian particles at 20°C (*4*). No self-driven flow was observed in tunnels created within PDMS—the microspheres exhibited active Brownian motion but no directional flow (movie S6).

A common feature shared among the various flows was the direction—always toward the region with larger cross section or volume. In compound tunnels with wider and narrower sections, the flow direction at the junction was consistently from the narrower to the wider part; at both ends of the tunnel, the microspheres exited into the outside bath. In tapered tunnels, the microspheres moved from the narrower end to the wider end (Fig. 3A). These observations fit the proton gradient hypothesis: Since the protons emerge from a surface interaction, narrower tunnels with higher surface-to-volume ratios should yield relatively higher proton concentrations. Thus, when a narrower tunnel lies in series with a wider tunnel, the proton gradient should point from the narrower to the wider section, as consistently observed.

To explore additional features of self-driven flow, we used a compound tunnel made in an agarose gel (Fig. 2C). Agarose was chosen for several advantageous features: mechanical strength, optical clarity, and extremely low swelling rate (which excludes tunnel volume change as a relevant factor). The compound tunnel configuration helped elucidate the flow direction. In this configuration, the flow could last for ~30 min until all the microspheres were excluded from the region of interest (ROI). (End-state flow dynamics are described in the Supplementary Materials.)

A signature feature of the self-driven flow mechanism is the utilization of radiant energy (*5*). We tested whether IR, the most effective part of electromagnetic spectrum for expanding the EZ (*15*), could provide the energy for self-driven flow. IR was applied to the system from an enveloping water bath, which, in turn, was warmed by a microscope-stage heater (Fig. 2D). The infrared output from the water bath could be varied by adjusting the stage temperature. We found that increased infrared energy substantially increased the flow velocity (Fig. 3B).

Infrared energy may increase the flow in two ways: by enhancing the water-hydrogel interaction, thereby generating protons at a higher rate; and by creating a higher temperature, thereby enhancing proton diffusion. The practical significance of IR utilization lies in its ubiquity. For biological entities in particular, IR can be both exogenous and endogenous. Approximately 50% of solar energy received by earth is in the form of IR (*25*); metabolic activities of living organisms generate thermal radiation (heat), which is essentially IR (*26*).

Another prediction of the proton-gradient hypothesis is that the flow should be faster in narrower tunnels. Assuming the proton-release rate per unit area of the annular EZ is spatially invariant, then, since reduced tunnel diameter means increased surface-to-volume ratio, a narrower tunnel should lead to a higher proton concentration in the core (see Fig. 3A). This results in a higher proton gradient (assuming the bath's proton concentration remains unchanged), which, in turn, should lead to faster flow in the narrower tunnels. We tested the effect of tunnel diameter by decreasing the diameter

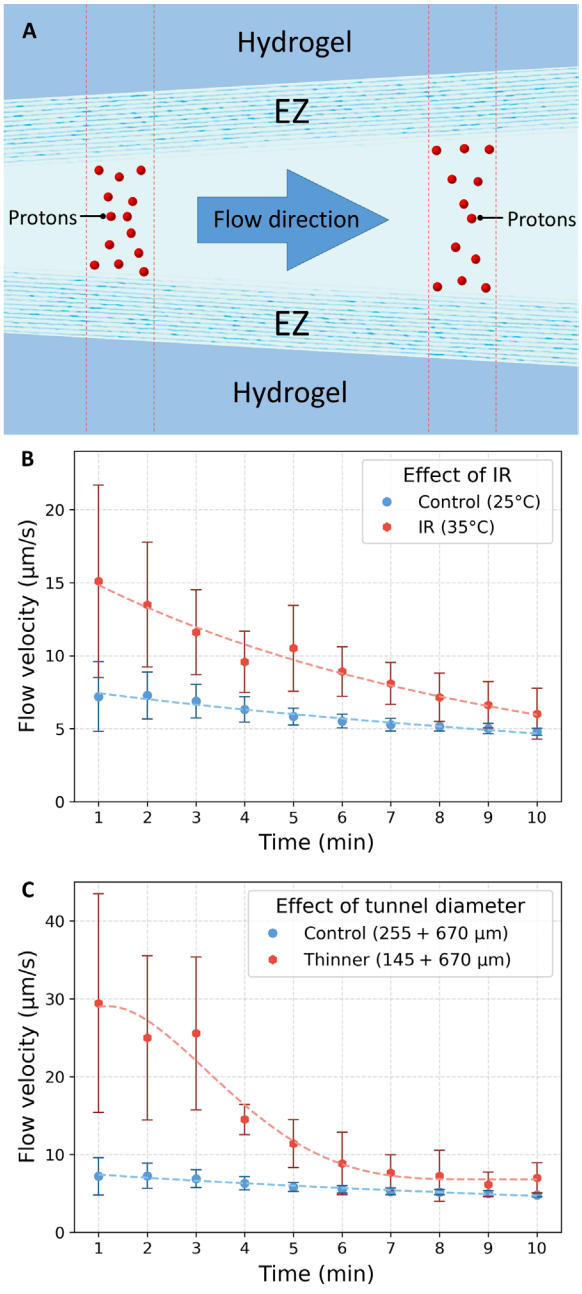

Fig. 3. Features of the self-driven flow. (**A**) The direction of the flow is toward the region with larger volume. EZ forms next to the tunnel wall. During formation, protons (red dots) are released into bulk water in the tunnel core. Narrower sections of the tunnel should have higher proton concentration than wider sections, forming a gradient pointing from narrower to wider. (**B**) Higher infrared radiation results in faster self-driven flow. Temperature in the legend indicates water bath temperature. (**C**) Smaller tunnel diameter results in faster self-driven flow. In both (B) and (C), $n = 5$; error bars denote SD.

of the narrower section of the tunnel (by using a thinner optical fiber as a mold), and the prediction was confirmed: Narrower tunnels produce faster flow (Fig. 3C). This is opposite of pressure-driven intratubular flow, where, by the Hagen-Poiseuille equation, narrower tunnels produce slower flow (*23*).

Features of material exchange–driven flow

With the generality of the self-driven flow confirmed, and an experimental model established, we moved to study another possibility: whether tubular flow could also be created through material exchange. This occurs when solvent/solutes enter/exit the tube through the tubular boundary, which occurs, for example, in capillaries of the circulatory system (*27*).

We studied one of the most common material exchange scenarios: water, the universal solvent, continuously exiting the tunnel through the tunnel boundary. An agarose gel, with compound tunnel, was chosen as a model. The experimental setup was almost identical to that of the self-driven flow study, except that the top surface of the gel was exposed to the air. With that exposure, the water continuously evaporated from the surface of the hydrogel. Evaporation increased hydrogel's osmotic pressure, which drew water from the tunnel into the gel.

With this model, we could again obtain flow. The flow appeared to contain two phases. Phase 1 was similar to the standard self-driven flow, as described above. After approximately 40 min, the pattern changed: The density of the microspheres decreased substantially; the EZ began diminishing in size and became less well defined; and the flow began to slow down and lastly reverse. Reversal denoted the onset of phase 2, where flows at the ends and at the junction all reversed direction. The reverse flow increased microsphere density, and the EZ disappeared (movie S7). Phase 2 flow continued so long as the microsphere suspension level stayed above the tunnel openings.

This two-phase flow may result from competition between the two proffered flow mechanisms—the self-driven flow and the material exchange–driven flow, the material in this case being water. Consider a compound tunnel inside a gel subjected to partial dehydration. The dehydrated gel draws water from the tunnel through the boundary. With the same initial osmotic pressure throughout the tunnel, the narrow region loses the water faster per unit volume due to that section's higher surface/volume ratio. In other words, the "water concentration" in the narrower section tends to decrease more rapidly than in the wider one. Thus, a "water concentration" potential gradient (or water potential gradient) forms, pointing from the wider region to the narrower region. This opposes the self-driven flow. For phase 1, the self-driven flow should dominate since the osmotic pressure of the hydrogel is still low. For phase 2, as more water evaporates from the gel surface, the tunnel's osmotic pressure increases. Once it dominates, the flow reverses.

For phase 2 flow, a higher IR input and a narrower tunnel size should enhance flow. A higher IR input increases gel temperature, which enhances evaporation and increases the gel's osmotic pressure, which results in faster flow. A narrower tunnel has a higher surface-to-volume ratio, generating a steeper water concentration gradient and then faster flow. These two expectations were confirmed (Fig. 4). A higher IR input and a narrower tunnel increased flow, during both stages.

Besides the solvent, solute exchange through the tunnel wall could create flow. In the Supplementary Materials, we provide an example demonstrating that a salt gradient across the tunnel wall can create an axial salt gradient in the tunnel, whose diffusion can create axial flow.

DISCUSSION

In sum, we report two mechanisms capable of generating intratubular flow in the absence of any pressure gradient. Self-driven flow exists

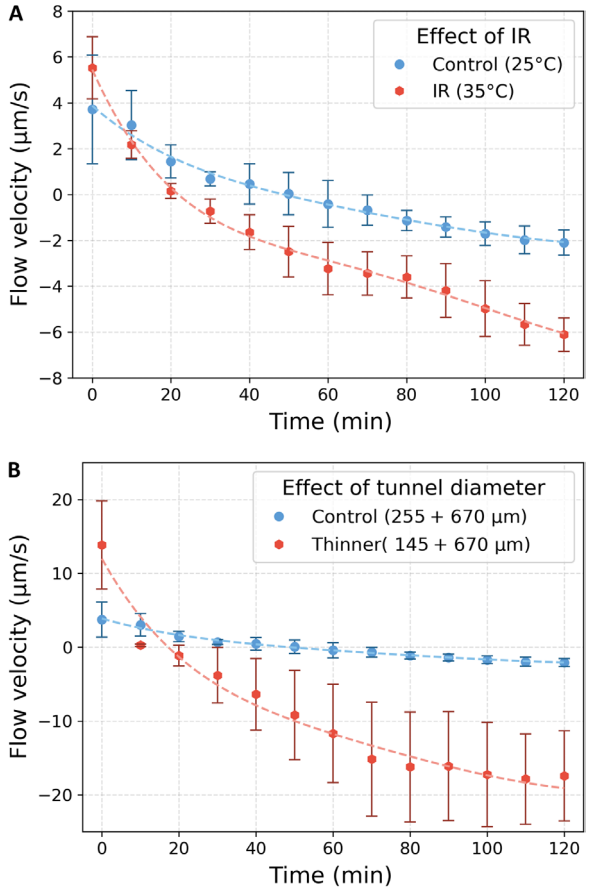

Fig. 4. Features of the material exchange-driven flow. Effect of IR (A) and tunnel size (B) on flow induced by material exchange (loss of water due to evaporation). (**A**) Elevated infrared energy resulted in faster flow. Temperature in the legend indicates water bath temperature. (**B**) Smaller tunnel diameter resulted in faster flow. Negative velocity denotes flow in the reverse direction (from a thicker to a thinner tunnel). In both (A) and (B), $n = 5$; error bars denote SD.

in tunnels lodged within diverse natural gels, driven by an axial proton gradient, the latter originating from a water-interface interaction. Material exchange through the boundary of the tunnel can cause material concentration gradients along the tube, also resulting in a flow. In both cases, the surface activities of the tunnel/tube boundary introduce a gradient into the tunnel/tube, which generates a flow. Hence, we suggest the generic name "surface-induced flow" (SIF).

Two features of SIF are distinct from those of pressure-driven flow: (i) IR energy augments the flow. Higher IR input enhances the water-interface interaction, which creates a larger proton gradient, thereby boosting the self-driven flow. In the material exchange mechanism, higher IR input increases the temperature, resulting in enhanced material exchange, larger axial material concentration gradients, similarly boosting the flow. (ii) SIF is more effective in narrower tunnels/tubes—opposite that of pressure-induced flow. This follows because the higher surface-to-volume ratio in narrower tubes facilitates this process.

The hydrogels used in this study are polymers with a large amount of water, carbon backbones, and different functional groups. The hydrogels generated EZs when dialyzed; however, the EZ behavior was not the same in the presence of extraneous ions. Agarose was observed to generate small-sized EZ, while EZ next to collagen was not visible under the microscope. We speculate that this difference in EZ behavior may arise from the functional groups in the hydrogel: Different groups interact with water differently. Extraneous ions in the hydrogel could combine with certain functional groups, changing the molecular structure in a way that inhibits the hydrogel-water interaction. The detailed nature of the hydrogel-water interaction, however, remains an outstanding question in the field.

The SIF mechanism may be important in both engineering and science. From the engineering perspective, SIF could be exploited for designing simple microfluidic pumps fueled by IR energy, which is freely available throughout the environment. From the science perspective, SIF may provide mechanistic understanding of natural fluid transport, particularly in biology.

SIF could be used by the circulatory system. Material exchange plays an important role in the circulatory system, especially in capillaries. Thus, material exchange–driven flow could facilitate circulation at the level of microcirculation. Regarding the self-driven flow mechanism, blood vessel interiors appear to be lined with EZs. The glycocalyx, a gel-like polysaccharide, lines the insides of vessels (*21*, *22*). Beyond the glycocalyx exists a cell-free layer that excludes red blood cells (*23*). The exclusion of red blood cells from an annular region inside the vessels implies the presence of an EZ, a seemingly critical feature for the existence of SIF. If SIF exists in the circulatory system, then we can make two predictions: (i) IR can be an energy source for blood circulation, and (ii) flow should persist even in the absence of cardiac contraction.

MATERIALS AND METHODS

Case and mold

The tunnel was built by molding. Hydrogel material was injected into a case fitted with a mold. After the hydrogel was cured, the molds were removed, leaving a tunnel within the gel.

Case, mold, and retainer used for agar, agarose, and collagen tunnels

The case holds the hydrogel. It was made from a polystyrene spectrophotometer cuvette. The top part of the cuvette was cut off, leaving only the bottom section, with dimensions of 1 cm by 1 cm by 0.6 cm (length by width by height). A hole was drilled on each of two opposite sides of the case to allow the insertion of the mold. The sizes of the holes were the same as the diameters of the molds, and the height of the holes to the floor of the case was determined by the working distance of the microscope.

The mold determined the geometry of the tunnel. The mold was assembled by inserting a piece of optical fiber into a needle. With this configuration, the tunnel was composed of a narrow and a wide region. The length of each region was equal, and the total length of the tunnel was 1 cm. Two tunnel geometries, control geometry, and narrow geometry, were built respectively to study the effect of tunnel diameter. For different geometries, different optical fibers were used for the narrow region, and the needle for the wide region remained the same.

- Needle: diameter = 670 μm [BD (Becton, Dickinson and Company), 305193], tip blunted by a rotary grinder.

- Optical fiber for control geometry: diameter = 255 μm (Corning, LNF 62.5/125).

- Optical fiber for narrow geometry: diameter = 145 μm (Nufern, CMF-P).

A retainer facilitated the removal of the mold. It was made from a polystyrene spectrophotometer cuvette and a glass slide. A hole

was drilled on each of the two opposite sides of the spectrophotometer cuvette. The size of the holes was the same as the diameter needle, and the location of the holes matched that of the case. The cuvette was then glued onto a glass slide. When the needle was being removed, the two holes on the retainer prevented the needle from wiggling.

To assemble the case, mold, and retainer, the optical fiber was first inserted into the case, and then the needle, which was fixed by the retainer, was inserted into the case. Thereafter, the optical fiber was inserted into the needle, all the way to the other side (fig. S1A). The junction of the optical fiber and the needle was set at the middle point of the prospective tunnel.

For agar, agarose, and collagen tunnels, no extra treatment was needed for the case and the mold before gel injection. For PDMS tunnels, trichloro(1*H*,1*H*,2*H*,2*H*-perfluoro-octyl)silane (Sigma-Aldrich, 448931-10G) was coated onto the case and mold to prevent the mold from sticking to PDMS. The coating was deposited by evaporation: One drop of silane was deposited onto a watch glass. The case, mold, and watch glass were placed in a desiccator. The desiccator was connected to the laboratory's vacuum system whose pressure was 41.1 kPa. The vacuum was on for 30 min. During this time, silane evaporated and coated the case and mold.

To remove the mold, first, the needle was rotated slowly to separate from the hydrogel/PDMS. Then, the optical fiber was slowly pulled away from the retainer side, and the needle was pulled away afterward. Removing the optical fiber first, before the needle, prevented hydrogel/PDMS debris being left in the tunnel. The hydrogel/PDMS tunnel remained in the case during all experiments.

Case and mold used for gelatin tunnel

A case was made from a 1-ml syringe (BD, 309623). The needle from this syringe/needle set was not used. The tip of the syringe was cut off, and two holes that allowed a tight fitting of the molds were drilled on the syringe wall, through the diameter of the cylindrical syringe. The plunger remained in the syringe, and the space formed by the plunger and the syringe wall was used to contain the hydrogel.

A thin needle, a piece of optical fiber, and a thick needle each composed of $^1/_3$ of tunnel length was used as mold (fig. S1B).

Mold:

- Thin needle: diameter = 670 μm (BD, 305193), tip blunted by a rotary grinder.

- Optical fiber for narrow geometry: diameter = 145 μm (Nufern, CMF-P).

- Thick needle: diameter = 1070 μm (CML Supply, 901-19-100).

The gelatin gel swelled greatly after dialysis. Thus, the tunnel-containing gel was removed from the case for dialysis. To remove the gel, the plunger was pushed, and the gel was softly scraped away with a spatula.

After dialysis, the tunnel diameter was larger than that of the mold due to swelling. The tunnel-containing gelatin gel was not placed back into any case for experiments.

Case and mold used for starch tunnel

To see the microspheres clearly through the opaque starch gel, a wider tunnel was built by using a thicker mold. Also, the distance between the gel surface and the tunnel was reduced by using less gel.

The case was made from a polystyrene spectrophotometer cuvette. The top part of the cuvette was cut off, leaving only the bottom section, with dimensions of 1 cm by 1 cm by 0.6 cm (length by width by height). A hole was drilled on each of two opposite sides of the case to allow the insertion of the mold. The size of the holes allowed a tight fitting of the mold, and height of holes to the floor of the case was determined by the working distance of the microscope.

A 20-μl pipette tip (Rainin, RT-L10FLR) was used as a mold. The setup is shown in fig. S1C. The starch tunnel remained in the case during all experiments.

DI water

The DI water used in all experiments was obtained from a DI water system (Barnstead, Nanopure analytical system, D11901). The resistivity of the DI water was 18.2 megohm·cm at 25°C.

Agarose

Agarose (Sigma-Aldrich, A6560) was mixed with DI water at a ratio of 1.5% (w/w) (0.6 g agarose/40 g water) in a 50-ml conical centrifuge tube (Corning, 352098). The tube was heated in a boiling water bath for 20 min. The mixture was then aliquoted to 2-ml microcentrifuge tubes (Eppendorf, 022363344) and stored at 4°C.

When needed, the aliquoted agarose was reheated in a boiling water bath for 2 min to melt. The liquefied agarose was immediately placed in a desiccator, cooled at atmospheric pressure for 1 min, and then degassed with the laboratory's vacuum system (41.4 kPa) for 1 min. After degassing, the liquefied agarose gel was injected into the case until full and solidified at 4°C for 8 min.

Agar

Agar (Sigma-Aldrich, A9799) was mixed with DI water at a ratio of 1.5% (w/w) (0.6 g agar/40 g water) in a 50-ml conical centrifuge tube (Corning, 352098). The tube was then heated in a boiling water bath for 20 min. The mixture was then aliquoted into 2-ml microcentrifuge tubes (Eppendorf, 022363344) and stored at 4°C.

When needed, the aliquoted agar was reheated in a boiling water bath for 2 min to melt. The liquefied agar was immediately placed in a desiccator, cooled at atmospheric pressure for 1 min, and then degassed with the laboratory's vacuum system (41.4 kPa) for 1 min. After degassing, the liquefied agar gel was injected into the case until full and solidified at 4°C for 8 min.

Starch

Hydrolyzed potato starch (Sigma-Aldrich, S5651) was mixed with DI water at a ratio of 40% (w/w) (1.2 g starch/3 g DI water). The mixture was added to 7 ml of boiling DI water contained in a 50-ml conical centrifuge tube (Corning, 352098) to form a thick starch gel suspension at a ratio of 12% (w/w) (1.2 g starch/10 g DI water) (*28*). The mixture was heated in a boiling water bath and stirred with a glass rod. After 20 min of heating, the gel was degassed briefly under a negative pressure of 41.1 kPa and then injected into the case. The starch gel was solidified at 4°C overnight.

Gelatin

Gelatin (Carolina, 86-4660) was mixed with DI water at a ratio of 15% (w/w) (6 g gelatin/40 g water) in a 50-ml conical centrifuge tube (Corning, 352098) and heated in a boiling water bath for 10 min. The mixture was then aliquoted to 2-ml microcentrifuge tubes (Eppendorf, 022363344) and stored at 4°C.

When needed, the aliquoted gelatin was reheated in a boiling water bath for 5 min to melt. The melted gelatin gel was injected into the case until full. The gel was then cooled at room temperature for 15 min to solidify.

Collagen

Collagen gel with a concentration of 5 mg/ml was made by diluting and cross-linking the stock collagen solution (type I collagen from rat tail, 8–10 mg/ml, BD, 354249). The stock collagen solution came suspended in 0.02 N acetic acid. The gel cross-linking began once the pH was adjusted to neutral (*24*).

A neutralizing agent was prepared to adjust the gel pH as well as to dilute the collagen concentration to the desired level. The neutralizing agent consisted of 10× phosphate-buffered saline (PBS) (pH 7.4) (Gibco, 70011-044), distilled water (Gibco, 15230-162), and 1 N NaOH (Fisher Chemical, SS266-1). The amounts of components were calculated based on the final concentration of collagen gel (5 mg/ml) and the concentration of the stock collagen solution (varied in different batches). For each batch, pilot experiments were conducted to determine the optimum recipe for the neutralizing agent. The amounts of NaOH and distilled water were adjusted until the pH of the collagen-neutralizing agent mixture matched the pH of 1× PBS, which was 7.4. The pH was measured by litmus paper. After finalizing the recipe, a bulk volume of the neutralizing agent was prepared, and the amounts of each component were confirmed by weighing with a scale. Preparing a bulk volume at one time reduced errors; also, weighing has less error than volume measurement. The neutralizing agent was stored at 4°C until use.

When needed, a desired amount of stock collagen was injected into a 2-ml microcentrifuge tube (Eppendorf, 022363344), and the neutralizing agent was added to the stock collagen thereafter. The amounts of stock collagen and neutralizing agent were confirmed by weighing. The mixture was homogenized by alternatively vortexing (VWR, Vortex-genie 2) and dipping the collagen-containing centrifuge tube into ice water. The ice water kept the temperature of the mixture low. Both vortexing and cooling extended for 10 s each, and this pair of processes was repeated six times (2 min in total).

After being mixed, the collagen was degassed at a negative pressure of 41.1 kPa for 5 min and then spun in a centrifuge (Fisher Scientific, 05-090-100) at 4°C for 5 min to remove the bubbles generated during mixing and vacuuming. Thereafter, 200 μl of collagen was injected into the mold immediately and cured at room temperature (21°C) for an hour.

Polydimethylsiloxane

PDMS was made from a silicone elastomer kit (Dow Corning, Sylgard 184). The base and the curing agent of the kit were well mixed at a ratio of 10:1, and then, the PDMS mixture was injected into the case. PDMS was cured by heating at 60°C for 5 hours. After mold removal, the PDMS tunnel was washed with detergent and rinsed with DI water. PDMS tunnels were reused since no difference in microsphere behavior was observed in new or old PDMS tunnels.

Hydrogel dialysis

Hydrogels were sometimes dialyzed against DI water to reduce ion concentration and allow full hydration. In exploring the existence of EZ, all the hydrogels were tested with and without dialysis. In all the quantitative studies exploring the two flow regimes, the agarose gel was not dialyzed.

The dialysis procedure depended on the gel type. For agar, agarose, and starch, the raw material was dialyzed in dialysis tubing (Thermo Scientific, 88242) before gelation (heating). For gelatin and collagen, the gel was dialyzed after gelation.

The duration of the dialysis was set by the value of water conductivity. Ideally, if the conductivity of water used in dialyzing cannot further increase after changing water regularly, then the dialysis can be considered complete. However, components of air may dissolve in DI water, thereby increasing water's conductivity. To exclude this change, an extra container was used as a reference to determine the end point, as follows.

Two mason jars, with a volume of 1 liter each, were used for dialyzing: One jar contained the hydrogel and DI water, while the other contained only DI water. Conductivity in both jars was tracked with a conductivity meter (Oakton, CON 100). The water was changed in both jars every 4 hours. The dialysis was considered complete when the conductivity of dialyzing water matched that of the reference water or remained unchanged after two consecutive water changing cycles.

Microsphere suspensions

Unless stated otherwise, in all experiments, the microsphere suspensions were made by mixing 1-μm nonfunctionalized polystyrene microspheres (Polysciences, 07310-15) with DI water at a ratio of 45 μl (1 drop)/15 ml. The microsphere-to-water volume ratio was 1 to 300.

However, for visualizing the EZ next to hydrogels under varied conditions, the following microsphere suspensions were also used:

1) One-micrometer polystyrene microspheres with amidine functional groups (Invitrogen, A37322). The ratio of microsphere to DI water was 45 μl (1 drop)/30 ml.

2) One-micrometer polystyrene microspheres with amino functional groups (Polysciences, 17010). The ratio of microsphere to DI water was 20 μl/15 ml.

3) One-micrometer polystyrene microspheres with carboxylate functional groups (Polysciences, 08226). The ratio of microsphere to DI water was 45 μl (1 drop)/15 ml.

4) One-micrometer silica microspheres (Polysciences, 24326-15). The ratio of microspheres to DI water was 40 μl/15 ml.

5) PDMS beads. The base and the curing agent of the PDMS kit (Dow Corning, Sylgard 184) were well mixed at a ratio of 10:1 (v/v) to form PDMS mixture. A 0.1% (v/v) Tween 20 (Sigma-Aldrich, P2287) and DI water solution was prepared. The PDMS mixture was mixed with this Tween 20 solution at a ratio of 10:1 (v/v). The mixture was shaken vigorously with a vortex mixer and placed at 60°C overnight to allow hardening into solid PDMS beads. The PDMS beads were then allowed to settle and then washed by replacing the supernatant with DI water. This washing procedure was carried out twice, to remove the surfactant (Tween 20) used during preparation (*29*). When used, the concentration of the PDMS-bead suspension was adjusted with DI water until the turbidity roughly matched that of polystyrene microsphere suspension.

6) Food-grade diatomaceous earth (Perma-Guard). The diatomaceous earth was well mixed with DI water at a concentration of 0.1% w/v and allowed to settle for 20 min. Larger particles settled down during this time. Only the supernatant was used for the experiment, because the size of diatomaceous earth particles in supernatant was comparable to that of polystyrene microspheres.

7) Food-grade active charcoal powder (Essential Elements). The carbon powder was well mixed with DI water at a concentration

of 0.04% w/v and allowed to settle for 20 min. Larger particles settled down during this time. Only the supernatant was used for the experiment, because the size of active charcoal powder in supernatant was comparable to that of polystyrene microspheres.

Applying IR

The thermal radiation from a water bath, heated by a heating stage beneath, was used as the IR source (fig. S2A). Using a water bath ensured uniform IR input around the petri dish. The level of IR output could be adjusted by appropriately adjusting the temperature of the water bath. The temperature of the heating stage could be stabilized to ±0.5°C, while the temperature of the water bath could be stabilized to ±0.1°C during the span of an experiment.

The heating stage was milled from an aluminum plate. Two film heating elements (Omega, KH-103/10-P) were attached to the bottom of the stage (fig. S2B). The power of the heating element, which determined the heating rate, was controlled by a power controller (Payne, 18TBP-1-15). The temperature of the heating element was controlled by a temperature controller (AGPtek, STC-1000). A temperature sensor read the temperature of the stage and provided feedback to the temperature controller.

The temperature controller turned on the heating element when the temperature was below the set point; when the temperature was above the set point, the heating element was turned off and the stage was cooled by ambient air. The power of the heating element was adjusted to a level that matched the cooling rate.

Observing self-driven flow

A glass petri dish (60 mm diameter by 15 mm height; Corning, 70165-60) containing 6 ml of DI water was used as water bath. A polystyrene petri dish (35 mm diameter by 15 mm height; Falcon, 351008) filled with 6 ml of microsphere suspension was placed in the water bath. For experiments with IR application, both water bath and microsphere suspension were preheated with the heating stage for 30 min before experiments.

After the tunnel was made, the microsphere suspension was injected into the tunnel with a 20-μl pipette through the larger opening on the case. Then, the tunnel was examined microscopically for any air bubbles inside. If necessary, the tunnel was flushed again until all bubbles were removed.

Next, the tunnel-containing case was placed in the middle of the petri dish containing the microsphere suspension. A drop of DI water was released onto the top surface of the gel, and then the surface was covered with a piece of glass coverslip. The glass coverslip stopped water from evaporating from the hydrogel, and the drop of DI water helped the glass slide to stick to the gel surface.

Further, the water bath and microsphere suspension were covered by a polystyrene petri dish lid to isolate the system from the environment as much as possible. Any water droplets deposited onto the lid appreciably diminishes image quality. Thus, a small observation window was opened on the lid (fig. S3).

A recording of the flow was obtained by using a video camera (Edmund Optics, EO-3112C), mounted on the microscope (Zeiss, Axiovert 100 TV) fitted with a 5× objective [numerical aperture (N.A.) = 0.13; Zeiss] and a 10× objective (N.A. = 0.25; Zeiss). To minimize interference with experimental protocols, the microscope light intensity was kept constant throughout all experiments.

Observing material exchange (solvent)–driven flow

We used the same configuration as for studying self-driven flow, except that the surface of the gel was exposed to the air.

Flow velocity quantification

The video recording of the flow was preprocessed by ImageJ (*30*). The preprocessing procedure included the following: (i) Splitting the video frames into segments of 20 s. Each data point is an average of 20 s of flow velocity. (ii) Cropping the regions of interest. (iii) Removing the background. The preprocessed data were then ready for analysis by PIV (*31*–*34*) to obtain the flow velocity.

Because of the presence of EZ, the region next to the tunnel wall is devoid of microspheres. Thus, only the middle part of the tunnel was used for data quantification.

SUPPLEMENTARY MATERIALS

Supplementary material for this article is available at http://advances.sciencemag.org/cgi/content/full/6/19/eaba0941/DC1

View/request a protocol for this paper from *Bio-protocol*.

REFERENCES AND NOTES

1. W. Harvey, *On the Motion of the Heart and Blood in Animals* (Prometheus Books, 1993).
2. R. Rushmer, in *Cardiovascular Dynamics* (Saunders, 1970), pp. 9–12.
3. R. K. Sinha, *Modern Plant Physiology* (Narosa, ed. 1, 2003).
4. A. Yu, P. Carlson, G. H. Pollack, Unexpected axial flow through hydrophilic tubes: Implications for energetics of water. *Eur. Phys. J. Spec. Top.* **223**, 947–958 (2014).
5. M. Rohani, G. H. Pollack, Flow through horizontal tubes submerged in water in the absence of a pressure gradient: Mechanistic considerations. *Langmuir* **29**, 6556–6561 (2013).
6. J.-M. Zheng, G. H. Pollack, Long-range forces extending from polymer-gel surfaces. *Phys. Rev. E Stat. Nonlin. Soft Matter. Phys.* **68**, 031408 (2003).
7. J.-M. Zheng, W.-C. Chin, E. Khijniak, E. Khijniak Jr, G. H. Pollack, Surfaces and interfacial water: Evidence that hydrophilic surfaces have long-range impact. *Adv. Colloid Interface Sci.* **127**, 19–27 (2006).
8. C.-S. Chen, W.-J. Chung, I. C. Hsu, C.-M. Wu, W.-C. Chin, Force field measurements within the exclusion zone of water. *J. Biol. Phys.* **38**, 113–120 (2012).
9. B. Chai, A. G. Mahtani, G. H. Pollack, Unexpected presence of solute-free zones at metal-water interfaces. *Contemp. Mater.* **3**, 1–12 (2012).
10. B. Sulbarán, G. Toriz, G. G. Allan, G. H. Pollack, E. Delgado, The dynamic development of exclusion zones on cellulosic surfaces. *Cellul.* **21**, 1143–1148 (2014).
11. D. Florea, S. Musa, J. M. R. Huyghe, H. M. Wyss, Long-range repulsion of colloids driven by ion exchange and diffusiophoresis. *Proc. Natl. Acad. Sci. U.S.A.* **111**, 6554–6559 (2014).
12. N. F. Bunkin, V. S. Gorelik, V. A. Kozlov, A. V. Shkirin, N. V. Suyazov, Colloidal crystal formation at the "Nafion–Water" interface. *J. Phys. Chem. B.* **118**, 3372–3377 (2014).
13. Y. Cheng, C. I. Moraru, Long-range interactions keep bacterial cells from liquid-solid interfaces: Evidence of a bacteria exclusion zone near Nafion surfaces and possible implications for bacterial attachment. *Colloids Surf. B Biointerfaces* **162**, 16–24 (2018).
14. J. Zheng, G. H. Pollack, in *Water and the Cell*, G. H. Pollack, I. L. Cameron, D. N. Wheatley, Eds. (Springer Netherlands, 2006), pp. 165–174.
15. B. Chai, H. Yoo, G. H. Pollack, Effect of radiant energy on near-surface water. *J. Phys. Chem. B* **113**, 13953–13958 (2009).
16. G. Pollack, *The Fourth Phase of Water* (Ebner & Sons, 2013), pp. 64–66.
17. J. M. Schurr, Phenomena associated with gel–water interfaces. Analyses and alternatives to the long-range ordered water hypothesis. *J. Phys. Chem. B.* **117**, 7653–7674 (2013).
18. J. M. Schurr, B. S. Fujimoto, L. Huynh, D. T. Chiu, A theory of macromolecular chemotaxis. *J. Phys. Chem. B.* **117**, 7626–7652 (2013).
19. G. H. Pollack, Comment on "A theory of macromolecular chemotaxis" and "Phenomena associated with gel–water interfaces. analyses and alternatives to the long-range ordered water hypothesis". *J. Phys. Chem. B.* **117**, 7843–7846 (2013).
20. P. Fratzl, in *Collagen: Structure and Mechanics*, P. Fratzl, Ed. (Springer US, 2008), pp. 1–13.
21. C.-B. Laurell, Quantitative estimation of proteins by electrophoresis in agarose gel containing antibodies. *Anal. Biochem.* **15**, 45–52 (1966).
22. C. R. Shaw, R. Prasad, Starch gel electrophoresis of enzymes—A compilation of recipes. *Biochem. Genet.* **4**, 297–320 (1970).
23. E. M. Ahmed, Hydrogel: Preparation, characterization, and applications: A review. *J. Adv. Res.* **6**, 105–121 (2015).

24. J. P. Morgan, P. F. Delnero, Y. Zheng, S. S. Verbridge, J. Chen, M. Craven, N. W. Choi, A. Diaz-Santana, P. Kermani, B. Hempstead, J. A. López, T. N. Corso, C. Fischbach, A. D. Stroock, Formation of microvascular networks *in vitro*. *Nat. Protoc.* **8**, 1820–1836 (2013).
25. ASTM, in *Standard Tables for Reference Solar Spectral Irradiances: Direct Normal and Hemispherical on 37° Tilted Surface* (ASTM International, 2012).
26. F. Vatansever, M. R. Hamblin, Far infrared radiation (FIR): Its biological effects and medical applications. *Photon. Laser. Med.* **4**, 255–266 (2012).
27. R. E. Klabunde, in *Cardiovascular Physiology Concepts* (Lippincott Williams & Wilkins, ed. 2, 2012), pp. 187–191.
28. P. B. Aebersold, G. A. Winans, D. J. Teel, G. B. Milner, F. M. Utter, Manual for starch gel electrophoresis: A method for the detection of genetic variation. *NOAA Tech. Rep. NMFS* **61**, 1–19 (1987).
29. A. J. Mach, J. H. Kim, A. Arshi, S. C. Hur, D. Di Carlo, Automated cellular sample preparation using a Centrifuge-on-a-Chip. *Lab Chip* **11**, 2827–2834 (2011).
30. C. A. Schneider, W. S. Rasband, K. W. Eliceiri, NIH image to ImageJ: 25 years of image analysis. *Nat. Methods* **9**, 671–675 (2012).
31. W. Thielicke, E. J. Stamhuis, PIVlab—towards user-friendly, affordable and accurate digital particle image velocimetry in MATLAB. *J. Open Res. Softw.* **2**, e30 (2014).
32. C. D. Meinhart, S. T. Wereley, J. G. Santiago, A PIV algorithm for estimating time-averaged velocity fields. *J. Fluids Eng.* **122**, 285–289 (2000).
33. P. Vennemann, K. T. Kiger, R. Lindken, B. C. W. Groenendijk, S. Stekelenburg-de Vos, T. L. M. ten Hagen, N. T. C. Ursem, R. E. Poelmann, J. Westerweel, B. P. Hierck, In vivo micro particle image velocimetry measurements of blood-plasma in the embryonic avian heart. *J. Biomech.* **39**, 1191–1200 (2006).
34. Q. Tseng, E. Duchemin-Pelletier, A. Deshiere, M. Balland, H. Guillou, O. Filhol, M. Théry, Spatial organization of the extracellular matrix regulates cell–cell junction positioning. *Proc. Natl. Acad. Sci. U.S.A.* **109**, 1506–1511 (2012).

Acknowledgments: We thank W. Kaminsky, R. J. Wilkes, H. Lai, K. Böhringer, and Q. Yu for discussions on the experimental design; D. Dabiri and W. H. Tien for help on PIV technique; Z. Wan, Y. Zhao, H. Liu, M. Kowacz, A. Sharma, R. Sharma, J. Wu, S. Ren, T. Ye, and L. Colton for comments on the manuscript; A. Pinhas for comments on the cover letter and revision; M. Cantwell for expediting the employment authorization of Z.L.; and R. Hua for help on designing figures and continuous support to Z.L. to finish this project. **Funding:** This work was supported by an NIH Transformative grant 5R01GM093842, by the SAGST Foundation, and by private support. **Author contributions**: Z.L.: Data curation, formal analysis, investigation, methodology, project administration, software, validation, visualization, writing—original draft, and writing—review and editing. G.H.P.: Conceptualization, funding acquisition, project administration, resources, supervision, writing—original draft, and writing—review and editing. **Competing interests**: The authors declare that they have no competing interests. **Data and materials availability**: All data needed to evaluate the conclusions in the paper are present in the paper and/or the Supplementary Materials. Additional data related to this paper may be requested from the authors.

Submitted 14 November 2019
Accepted 24 February 2020
Published 8 May 2020
10.1126/sciadv.aba0941

Citation: Z. Li, G. H. Pollack, Surface-induced flow: A natural microscopic engine using infrared energy as fuel. *Sci. Adv.* **6**, eaba0941 (2020).

Surface-induced flow: A natural microscopic engine using infrared energy as fuel

Zheng Li and Gerald H. Pollack

Sci Adv **6** (19), eaba0941.
DOI: 10.1126/sciadv.aba0941